A numerical investigation of the influence of yarn-level finite-element model on energy absorption by a flexible-fabric armour during ballistic impact

M Grujicic[1]***, G Arakere**[1]**, T He**[1]**, M Gogulapati**[1], and **B A Cheeseman**[2]
[1]International Centre for Automotive Research CU-ICAR, Department of Mechanical Engineering, Clemson University, Clemson, South Carolina, USA
[2]Army Research Laboratory, Survivability Materials Branch, Aberdeen Proving Ground, Maryland, USA

The manuscript was received on 26 February 2008 and was accepted after revision for publication on 20 May 2008.

DOI: 10.1243/14644207JMDA209

Abstract: A series of transient non-linear dynamic finite-element method (FEM) analyses pertaining to the interaction of a single-ply plain-woven balanced square textile-fabric armour with a spherical steel projectile is carried out in order to compare the corresponding results obtained for two different yarn models: (a) a solid FEM model in which the warp and weft yarns are represented using first-order three-dimensional solid elements and (b) a membrane model in which the same yarns are represented using second-order membrane elements. The analyses are carried out under different yarn–yarn and projectile–fabric frictional conditions and under different far-field boundary conditions applied to the edges of the fabric. The results obtained showed that the two sets of analyses yield comparable predictions regarding the temporal evolution and the spatial distribution of the deformation and damage fields within the fabric, regarding the ability of the fabric to absorb the projectile's kinetic energy and regarding the relative contributions of the main energy absorbing mechanisms. The work also confirmed the roles yarn–yarn and projectile–fabric friction play in the impact process as well as the effect of the far-field boundary conditions applied to the edges of the fabric.

Keywords: flexible armour, high-performance fibres, ballistic performance

1 INTRODUCTION

Fibre-based materials and material systems used in lightweight body armour applications have been subjects of intense research and development efforts over the last half-century. These efforts have further intensified since the terrorist attacks of 11 September 2001. The most effective body armour currently used by military and law enforcement personnel is based on multiply fabrics and flexible fibrous composites. These are often supplemented by a hard and light ceramic strike-face plate (e.g. 5–10 mm thick B_4C plates) of which the primary role is to help blunt, erode, and/or fragment armour-piercing rounds. The same fibre-based materials are also critical components in the more-rigid armour panels used for ballistic protection of VIP automobiles, light military vehicles, helicopters, and airline cockpit doors.

Over the last several decades major advances have been made in the areas of development and fabrication of fibre-based materials for ballistic protection. Prior to the early 1970s, *poly-amide* (nylon) fibres dominated these classes of materials and their defining features were pronounced stress–strain non-linearities and relatively large strains-to-failure. Since then, new polymeric fibrous materials have been developed with substantially improved strength, stiffness, and ballistic performance. Among these high-performance fibres the most notable are: (a) *poly-aramids* (e.g. Kevlar®, Twaron®, and Technora®); (b) highly-oriented *poly-ethylene* (e.g. Spectra® and Dyneema®); (c) *poly-benzobis-oxazole* (PBO) (e.g. Zylon®); and (d) *poly-pyridobisimi-dazole* (PIPD)

**Corresponding author: International Centre for Automotive Research CU-ICAR, Department of Mechanical Engineering, Clemson University, 241 Engineering Innovation Building, Clemson 29634, South Carolina, USA.*
email: mica@ces.clemson.edu; mica.grujicic@ces.clemson.edu

Report Documentation Page

Form Approved
OMB No. 0704-0188

1. REPORT DATE	2. REPORT TYPE	3. DATES COVERED
2008		**00-00-2008 to 00-00-2008**

4. TITLE AND SUBTITLE
A numerical investigation of the influence of yarn-level finite-element model on energy absorption by a flexible-fabric armour during ballistic impact

5a. CONTRACT NUMBER
5b. GRANT NUMBER
5c. PROGRAM ELEMENT NUMBER

6. AUTHOR(S)

5d. PROJECT NUMBER
5e. TASK NUMBER
5f. WORK UNIT NUMBER

7. PERFORMING ORGANIZATION NAME(S) AND ADDRESS(ES)
Celmson University,Department of Mechanical Engineering,Clemson,SC,29634

8. PERFORMING ORGANIZATION REPORT NUMBER

9. SPONSORING/MONITORING AGENCY NAME(S) AND ADDRESS(ES)

10. SPONSOR/MONITOR'S ACRONYM(S)
11. SPONSOR/MONITOR'S REPORT NUMBER(S)

12. DISTRIBUTION/AVAILABILITY STATEMENT
Approved for public release; distribution unlimited

13. SUPPLEMENTARY NOTES

14. ABSTRACT

A series of transient non-linear dynamic finite-element method (FEM) analyses pertaining to the interaction of a single-ply plain-woven balanced square textile-fabric armour with a spherical steel projectile is carried out in order to compare the corresponding results obtained for two different yarn models: (a) a solid FEM model in which the warp and weft yarns are represented using first-order three-dimensional solid elements and (b) a membrane model in which the same yarns are represented using second-order membrane elements. The analyses are carried out under different yarn?yarn and projectile?fabric frictional conditions and under different far-field boundary conditions applied to the edges of the fabric. The results obtained showed that the two sets of analyses yield comparable predictions regarding the temporal evolution and the spatial distribution of the deformation and damage fields within the fabric, regarding the ability of the fabric to absorb the projectile?s kinetic energy and regarding the relative contributions of the main energy absorbing mechanisms. The work also confirmed the roles yarn?yarn and projectile?fabric friction play in the impact process as well as the effect of the far-field boundary conditions applied to the edges of the fabric.

15. SUBJECT TERMS

16. SECURITY CLASSIFICATION OF:			17. LIMITATION OF ABSTRACT	18. NUMBER OF PAGES	19a. NAME OF RESPONSIBLE PERSON
a. REPORT	b. ABSTRACT	c. THIS PAGE			
unclassified	**unclassified**	**unclassified**	**Same as Report (SAR)**	**18**	

(e.g. M5®). When tested in tension, all these materials differ significantly from the nylon fibres, having very high absolute stiffness, extremely high specific strength (a ratio of strength and mass density), and quite low (<4 per cent) strains-to-failure. These fibres essentially behave, in tension, as rate-independent linear elastic materials. When tested in transverse compression, however, these fibres are similar to nylon and can undergo large plastic deformation without a significant loss in their tensile load-carrying capacity. This behaviour is quite different from that found in carbon or glass fibres, which tend to shatter under transverse compression loading conditions. Among the polymeric fibres mentioned, the best performer, PBO, has a tensile strength of ∼5 GPa (i.e. more than three times the tensile-strength of the strongest '*piano-wire*' steel but at a one-fifth of the steel density, resulting in an ∼15-fold higher density-normalized strength).

As mentioned, fabrics based on high-performance fibres are extensively employed in a variety of ballistic and impact protection applications. Despite the fact that over the past two decades there has been a great deal of work done on understanding the ballistic behaviour of these fabrics using various analytical and numerical techniques, the design of fabric armour systems remains largely based on the employment of extensive experimental test programs, empiricism, and old practices. While such experimental programs are critical for ensuring the utility and effectiveness of the armour systems, they are generally expensive, time-consuming, and involve destructive testing. Consequently, there is a continual effort to reduce the extent of these experimental test programs by complementing them with the corresponding computation-based engineering analyses and simulations.

Among the main computational engineering analyses used to model ballistic performance of flexible armour the following classes can be identified.

1. Finite-element analyses based on the use of pin-jointed orthogonal bars to represent flexible-fabric yarns. The most notable studies falling into this category of analyses are those performed by Roylance and Wang [**1**], Shim *et al.* [**2**], Lim *et al.* [**3**], Shahkarami *et al.* [**4**], Johnson *et al.* [**5**], and Billon and Robinson [**6**]. While the pin-jointed orthogonal-bars-based finite-element analyses have proved to be very efficient in approximating the dynamic behaviour of woven fabrics, the discrete nature of the yarn models was associated with inherent oversimplifications that significantly limited the predictive capability of the analyses. In particular, important contributions associated with the weave architecture, surface-finish, and friction governed yarn–yarn and layer-to-layer contacts (in multi-layer fabrics) could not be accounted for.
2. More-detailed full-blown three-dimensional continuum finite-element analyses, such as those carried out by Shockey *et al.* [**7**], Duan *et al.* [**8–11**], and Zhang *et al.* [**12**], etc. While these analyses have proved to be powerful tools for capturing and elucidating the detailed dynamic response of single-layer fabrics, they are computationally very demanding when applied to practical armour systems that typically contain 30–50 fabric layers per ply.
3. Unit-cell based approaches have been used extensively in order to derive the equivalent (smeared) continuum-level (membrane/shell) material models of textile composites from the knowledge of the meso-scale fibre and yarn properties, fabric architecture, and inter-yarn and inter-ply frictional characteristics. Among the most notable studies based on these analyses are those carried out by Kawabata *et al.* [**13–15**] who introduced simple analytical models to capture the uniaxial, biaxial, and shear behaviour of fabrics. Furthermore, Ivanov and Tabiei [**16**] proposed a micro-mechanical material model for a woven fabric (in which a visco-elastic constitutive model was used to represent the mechanical behaviour of the yarns) for use in non-linear finite-element impact simulations. In deriving the material model, Ivanov and Tabiei [**16**] considered the motion of the yarn-crossover point and developed a procedure for determining the equilibrium position of this point under the applied unit-cell strains. Recently, King *et al.* [**17**] proposed a new approach for deriving the continuum-level material model for fabrics, based on the properties of the yarns and the weave architecture, which involves the use of an energy minimization technique to establish the relationship between the configuration of the fabric structure and the microscopic deformation of fabric components. Similar unit-cell based continuum-level membrane/shell material models have been developed by Boisse *et al.* [**18**] and Peng and Cao [**19**]. Also, Shahkarami and Vaziri [**20**] proposed a model similar to but simpler than that introduced by King *et al.* [**17**] and provided a detailed account of its incorporation into a material-model subroutine that can be readily coupled with commercial dynamic-explicit finite-element codes.
4. The use of higher-order membrane/shell finite-element analyses to represent the dynamic response of the fabric under ballistic loading conditions and overcome the aforementioned computational cost associated with the use of full three-dimensional finite-element analyses of the yarn/fabric structure. Among the studies falling into this category, the most notable is the one carried out by Scott and Yen [**21**]. While the use of higher order membrane elements was found

to be indeed advantageous computationally, it was never fully validated by comparing its results against either those obtained experimentally or those obtained using full three-dimensional finite-element analyses.

5. As mentioned earlier, full-blown three-dimensional finite-element models used in the simulations of ballistic performance of textile armour systems are quite powerful but become computationally rather expensive when applied to commercial multi-ply flexible-armour systems. On the other hand, higher-order membrane models for flexible armour systems are computationally advantageous and offer the possibility of carrying out the finite-element analysis of ballistic performance of commercial multi-ply flexible armour systems. However, the validity/reliability of the higher-order membrane models was never fully validated. Hence, the main objective of this work is to carry out a parallel investigation of the ballistic performance of a prototypical single-ply plain-woven balanced square flexible-textile armour using both full-blown three-dimensional and higher-order membrane models of the flexible armour.

The article is organized as follows. The details regarding the computational procedures employed in this work in deriving the yarn-level material properties, fabric architectures, and the formulation of a transient non-linear dynamics problem pertaining to the impact of a single-ply plain woven balanced fabric armour with a spherical projectile are overviewed in section 2. The main results obtained in the current work are presented and discussed in section 3. The principal points and conclusions resulting from this work are listed in section 4.

2 COMPUTATIONAL PROCEDURE

This section provides a more detailed description of the finite-element analyses that were used to study the effect of the impact of a spherical projectile onto single-ply plain-woven square flexible textile armour.

2.1 Material model

In this paper, the fabric is modelled at a yarn-level resolution, i.e. warp and weft yarns are assumed to be made of continuum-type material. In other words, no account of the fibre length-scale material effects within the yarns is taken. The yarn material is considered to be orthotropic (more precisely, transversely isotropic) linear-elastic material up to the point of fracture. Since the fibres within yarns are aligned in the yarn-length direction, this direction is associated with the highest levels of stiffness. To account for the fact that yarns are made of bundled fibres and that, consequently, fibres juxtaposition can readily take place during transverse and shear loading, all shear moduli and Poisson's ratios are set to very small values and, likewise, the transverse Young's moduli are taken to be a small fraction of the longitudinal (along the yarn length) Young's modulus. A summary of the yarn-level orthotropic linear elastic material properties for Kevlar-129® fibre-based yarns used in this work was taken from reference [**11**] and is given in Table 1. One might expect that in the absence of binding resin, the shear moduli of the yarn should be lower than their values shown in Table 1. Nevertheless, these values are reasonable and they reflect the effect of inter-fibre friction within the yarns. In addition to the linear-elastic orthotropic material properties given in Table 1, and in accordance with the limited-ductility and brittle nature of the constituent high-performance Kevlar-129 fibres, failure of the yarns is assumed to be strain controlled (i.e. to take place when the strain along the yarn length reaches a critical value, the failure stain of 4 per cent).

Table 1 The orthotropic elastic material data (GPa) for yarn [**11**]

E_{11}	E_{22}	E_{33}	G_{12}	G_{13}	G_{23}	N_{12}	N_{13}	N_{23}
164	3.28	3.28	3.28	3.28	3.28	0	0	0

2.2 Fabric architecture and yarn discretization into finite elements

As mentioned earlier, the fabric is modelled at the yarn-level resolution, i.e. the warp and the weft yarns are woven to produce a plain-woven balanced fabric. Two types of finite-element methods/discretizations (FEM) are considered: (a) first-order eight-node solid-brick elements are used to represent the yarns (referred to the solid FEM analysis) and (b) second-order eight-node membrane elements are used to discretize the yarn (referred to as the membrane FEM analysis). These two analyses are discussed in more detail here.

2.2.1 Solid FEM model

A typical three-dimensional FEM model for the fabric used in this work is displayed in Fig. 1(a). For both warp and weft yarns, a side-truncated sinusoidal cross-sectional area was assumed, which remains constant along the yarn length. Typical values for the yarn-crimp wavelength of 1.64 mm, the volumetric density of the fabric of 600 kg/m^3, and the fabric thickness of 0.23 mm are assumed. The yarn cross-section is discretized using 12 elements and one yarn wavelength

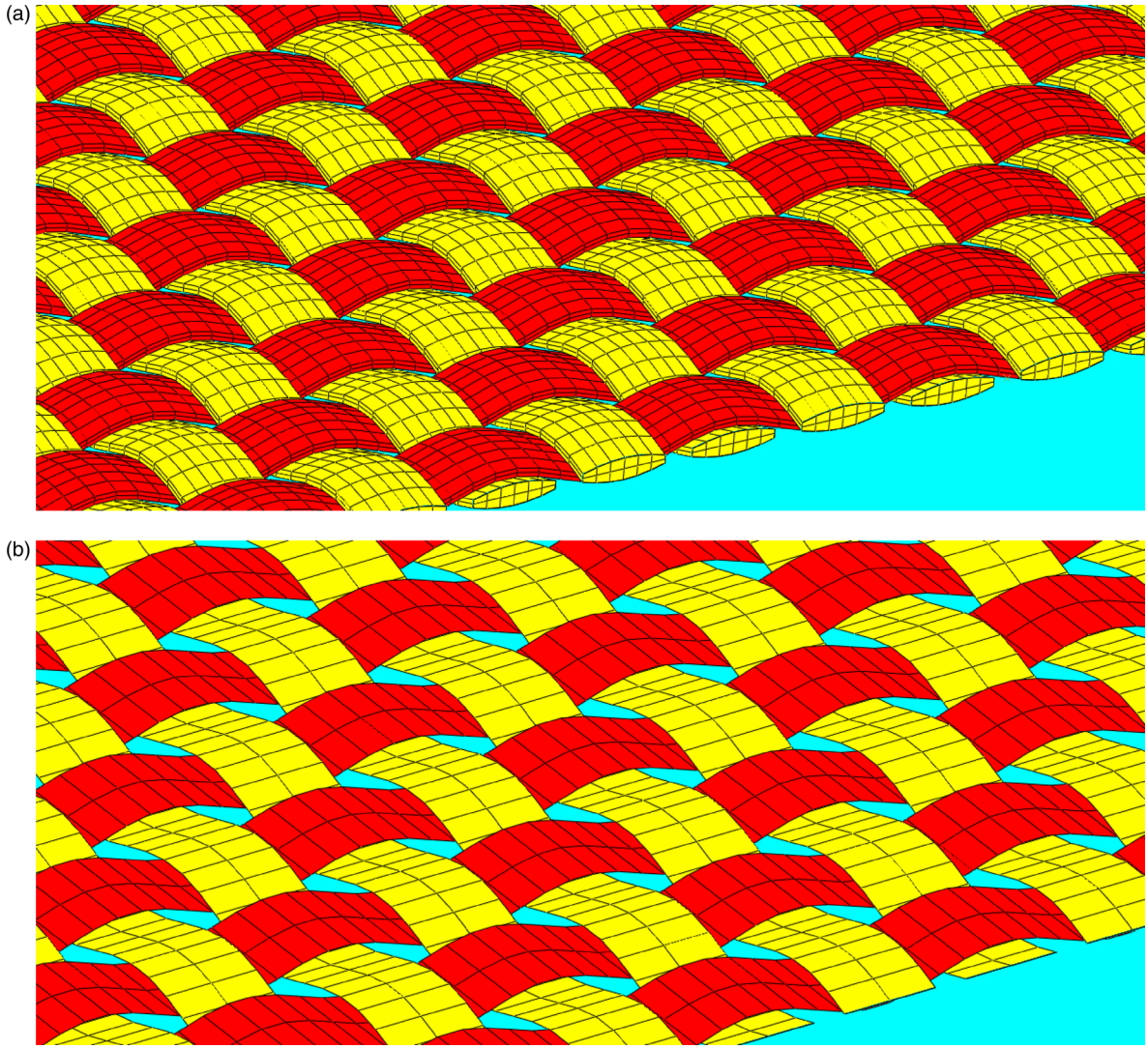

Fig. 1 Three-dimensional finite-element models of a plain-woven simple-ply balanced textile-fabric armour: (a) first-order eight-node solid finite-element representation and (b) the corresponding second-order eight-node membrane representation

is discretized using ten elements. Typically, a solid FEM model contained ∼200 000 first-order eight-node solid-brick elements, ∼350 000 nodes, and ∼1 000 000 degrees of freedom.

2.2.2 Membrane FEM model

A typical membrane FEM model used in this work is displayed in Fig. 1(b). The same fabric architecture as in the case of the solid FEM model was used. Yarns were discretized using second-order eight-node membrane elements. To account for the variable yarn thickness along its cross-section, a 'Nodal Thickness' option was used within ABAQUS/Explicit. Typically the membrane FEM model consisted of ∼36 000 second-order eight-node membrane elements, ∼50 000 nodes, and ∼300 000 degrees of freedom.

2.3 Impact of the fabric by a spherical projectile problem definition

In both the FEM analyses discussed, the same type of 2.1 g solid steel spherical projectile with a 4 mm-radius and an initial velocity of 100 m/s were used. The projectile is modelled as a rigid body consisting of 2095 tetrahedron elements whose all degrees of freedom but one (the translational degree of freedom normal to the fabric) are constrained. Figure 2 shows the initial configuration of the projectile–fabric system for the solid FEM model. The corresponding initial configuration for the membrane FEM model is quite similar to that displayed in Fig. 2 and is not shown for the sake of brevity.

Yarn–yarn and projectile–fabric contacts are modelled using a robust hard-contact–penalty algorithm provided by the ABAQUS/Explicit finite-element

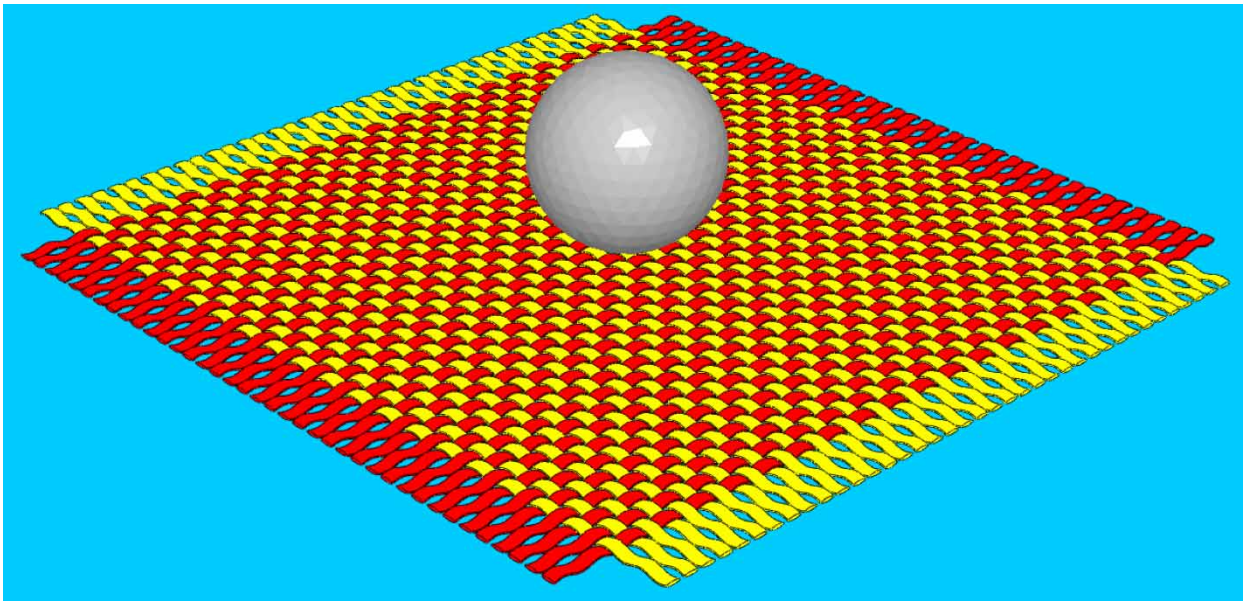

Fig. 2 The initial configurations of the projectile–fabric system for the solid FEM analysis

program [**22**] used in this work. Also, a simple Coulomb friction model was used to account for the yarn–yarn and projectile–fabric frictional effects. Four frictional conditions were considered: (a) both the yarn–yarn friction coefficient $\mu_{y/y}$ and the projectile–fabric friction coefficient $\mu_{p/f}$ are set to 0.5; (b) no friction; (c) $\mu_{y/y} = 0.5$ and $\mu_{p/f} = 0$; and (d) $\mu_{y/y} = 0$ and $\mu_{p/f} = 0.5$.

Three different types of boundary conditions for the edges of the fabric are considered: (a) all four edges are clamped; (b) two opposite edges are clamped and the other two are free; and (c) all four edges are free except that the four corner nodes are fixed.

To prevent hour-glassing effects that may arise due to the use of reduced-integration elements, a default value of hour-glass stiffness was used. No instability-type problems were encountered and hence no mass-scaling algorithm was used to control the maximum stable time increment.

2.4 Projectile-to-fabric energy transfer during ballistic impact

Since one of the key ballistic-performance requirements of an armour system is to absorb the kinetic energy carried by the impacting projectile, a brief overview of the major projectile-to-fabric energy transfer mechanisms during impact is presented in this section. The impact of a projectile with the fabric is associated with the initiation of several phenomena, the most important of which are: (a) a resisting force is exerted by the fabric onto the projectile, which causes a reduction in the projectile velocity; (b) at the same time, the fabric is being deformed and accelerated; and (c) strain waves generated in the impact region propagate along the yarns toward the fabric edges, where they are reflected. In the absence of any external force acting on the projectile–fabric system, the total energy of the system must be conserved. In general, the energy dissipation due to projectile deformation, fibre intermolecular friction, wind resistance, and acoustic losses are all assumed to be negligible. Consequently, any loss in projectile kinetic energy ΔE_{pk} can be mainly attributed to the following three energy-absorbing mechanisms: strain energy acquisition by the yarns E_{ys}, kinetic energy acquisition by the yarns E_{yk}, and the energy loss due to frictional sliding at the yarn–yarn and projectile–fabric contact surfaces E_f. The energy conservation principle then requires that

$$\Delta E_{pk} = E_{ys} + E_{yk} + E_f \tag{1}$$

As clearly shown by Duan *et al.* [**8–11**], the loss of projectile kinetic energy ΔE_{pk} is governed (through the three aforementioned energy-absorption mechanisms) by several factors such as the material properties of the constituent fibres, fabric structure, boundary conditions, projectile geometry, impact velocity, friction between the projectile and the fabric, and yarn–yarn and fibre-to-fibre friction within the fabric itself.

Traditionally, the overall decrease in projectile kinetic energy (ΔE_{pk}) is determined using ballistic impact experiments in which only the projectile initial velocity (v_i) and the residual velocity (v_r) are measured. The overall decrease in projectile kinetic energy (ΔE_{pk}) is then defined as

$$\Delta E_{pk} = \frac{1}{2} m[v_i^2 - v_r^2] \tag{2}$$

where m is the mass of the projectile. Recently, Starratt *et al.* [**23**] developed a ballistic-impact method for continuous measurement of projectile velocity $\upsilon(t)$. The loss of projectile kinetic energy as a function of time t during impact is then defined as

$$\Delta E_{\mathrm{pk}} = \frac{1}{2} m[\upsilon_{\mathrm{i}}^2 - \upsilon(t)^2] \tag{3}$$

While this experimental technique may greatly help to improve our understanding of the ballistic impact behaviour of fabrics, at the present time, many essential physical phenomena accompanying projectile–fabric interactions can only be revealed using numerical analyses and simulations like those used in this work.

3 RESULTS AND DISCUSSION

In this section, selected results are shown and discussed with the main emphasis placed on establishing if the computationally more efficient second-order membrane FEM analyses can be used in place of the more accurate yet computationally more demanding solid FEM analyses to study the impact of flexible textile armour with high-velocity projectiles. Since it is well established that yarn–yarn and projectile–fabric friction and the far-field boundary conditions applied to the edges of the flexible textile armour may play important roles in the ability of the armour to absorb the kinetic energy of the projectile, different friction conditions and far-field boundary conditions were considered in this work. It should be noted that the work of Cheeseman and Bogetti [**24**] established that not only the far-field boundary conditions, yarn–yarn friction and projectile–fabric frictions but also other factors such as material properties of the fibres and yarns, fabric structure/architecture, and projectile geometry and velocity may affect the ability of armour to defeat the projectile. These additional factors were either not considered in this work (e.g. fibre/yarn material properties, fabric structure/architecture, and projectile velocity) or were analysed but the results are not shown since they are consistent with the results given in this paper (e.g. the effect of projectile, spherical versus cylindrical geometry).

Since the key functional requirement for an armour system is to absorb the kinetic energy carried by the projectile, a quantitative comparison of the results pertaining to the temporal evolution of the absorbed energies (through yarn deformation and fracture, fabric acceleration, and frictional-sliding based energy dissipation) obtained using the solid FEM and the membrane FEM analyses is carried out in the subsequent sections. The results obtained for the case of far-field boundary conditions corresponding to all four fabric edges being clamped, for all four frictional conditions and for the spherical shape of the projectile is discussed in the next section. The effects of the type of the far-field boundary conditions and the projectile (spherical versus cylindrical) shape are then discussed in the subsequent two sections, respectively.

3.1 Four-edges clamped far-field boundary conditions

The results presented in this section correspond to the case of fixed boundary conditions applied to all four edges of the fabric. As discussed earlier, yarn–yarn friction and projectile–fabric friction are generally present in experimental and field tests of flexible-fabric armour and as shown by Tan *et al.* [**25**] in a series of post-impact fabric-inspection studies, and play an important role in absorbing the projectile kinetic energy (e.g. yarn-crossover domains near the impact region are found to be characterized by extensive fibre breakage and, in the absence of friction, substantial slippage is observed between the warp and weft yarns while the impact-induced fabric-perforation is typically smaller than the projectile size). Consequently, the first case analysed here is the one in which both the yarn–yarn friction coefficient $\mu_{\mathrm{y/y}}$ and the projectile–fabric friction coefficient $\mu_{\mathrm{p/f}}$ are set to a non-zero (=0.5) value.

3.1.1 Fabric deformation and yarn fracture

Examples of the temporal evolution of deformation within the fabric obtained using the solid FEM and the membrane FEM analyses are displayed in Figs 3 and 4, respectively, where side and top views of the fabric along with superimposed contour plots of the transverse displacement (the displacement normal to the fabric surface) are shown. A simple comparison of the results displayed in Figs 3 and 4 reveals that the temporal evolution of the deformation state of the fabric is quite similar in the two analyses and can be summarized as in the list.

1. Up to ∼16 μs, the shape of the transverse-deflection wave front in the fabric is nearly circular and, thus, essentially identical to the shape of the projectile–fabric contact-zone.
2. As time proceeds, the transverse-deflection wave generated within the principal yarns (the yarns that are in direct contact with the projectile) propagates outward and, through its interaction with the secondary yarns (the yarns which are not in direct contact with the projectile) at the yarn crossovers, causes the secondary yarns to also deflect in the transverse direction. Consequently, at ∼30–35 μs, the transverse-wave front begins to acquire a near square shape, with the square centre coinciding with the impact-zone centre.

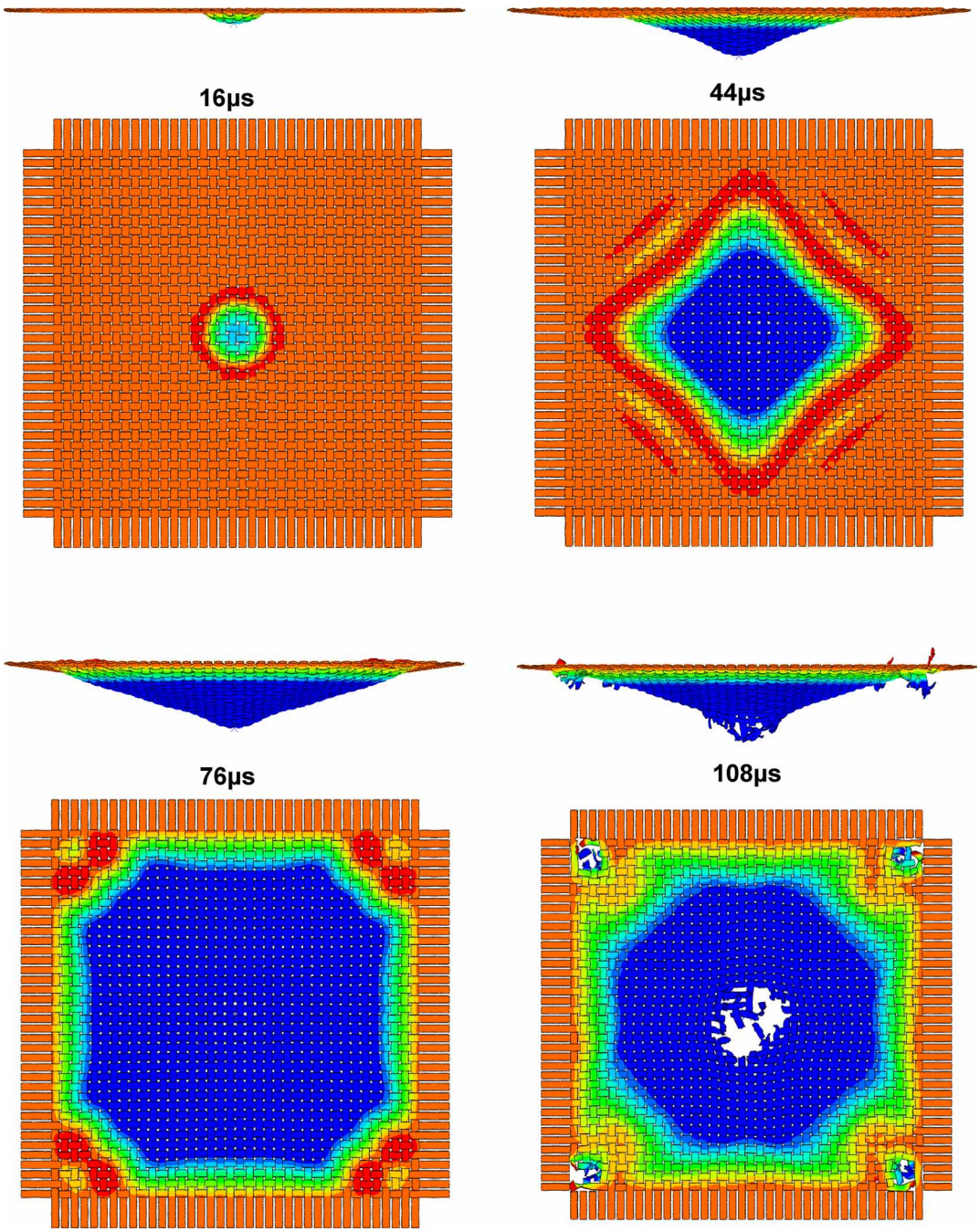

Fig. 3 The temporal evolution of deformation in the fabric for the solid FEM model under the yarn–yarn and projectile–fabric friction-coefficient conditions of 0.5. Contour bands correspond to different values of the transverse displacement, i.e. the displacements normal to the fabric surface

3. The square-shaped transverse wave continues to propagate towards the clamped edges of the fabric and, upon reaching the edges at ∼60–65 μs, it is reflected back towards the centre of the impact zone and the wave front acquires an octagonal shape.
4. At ∼100–105 μs, the projectile completely penetrates the fabric and continues to move at a residual velocity of 26 m/s in the case of solid FEM analysis and at a velocity of 28 m/s in the case of membrane FEM analysis. In the case of the solid FEM analysis fabric failure is also observed at the four corners of the clamped fabric patch. A similar fabric-corner failure mode was also observed in the case of membrane FEM analysis but at rather (>10 per cent) higher projectile velocities (the results not

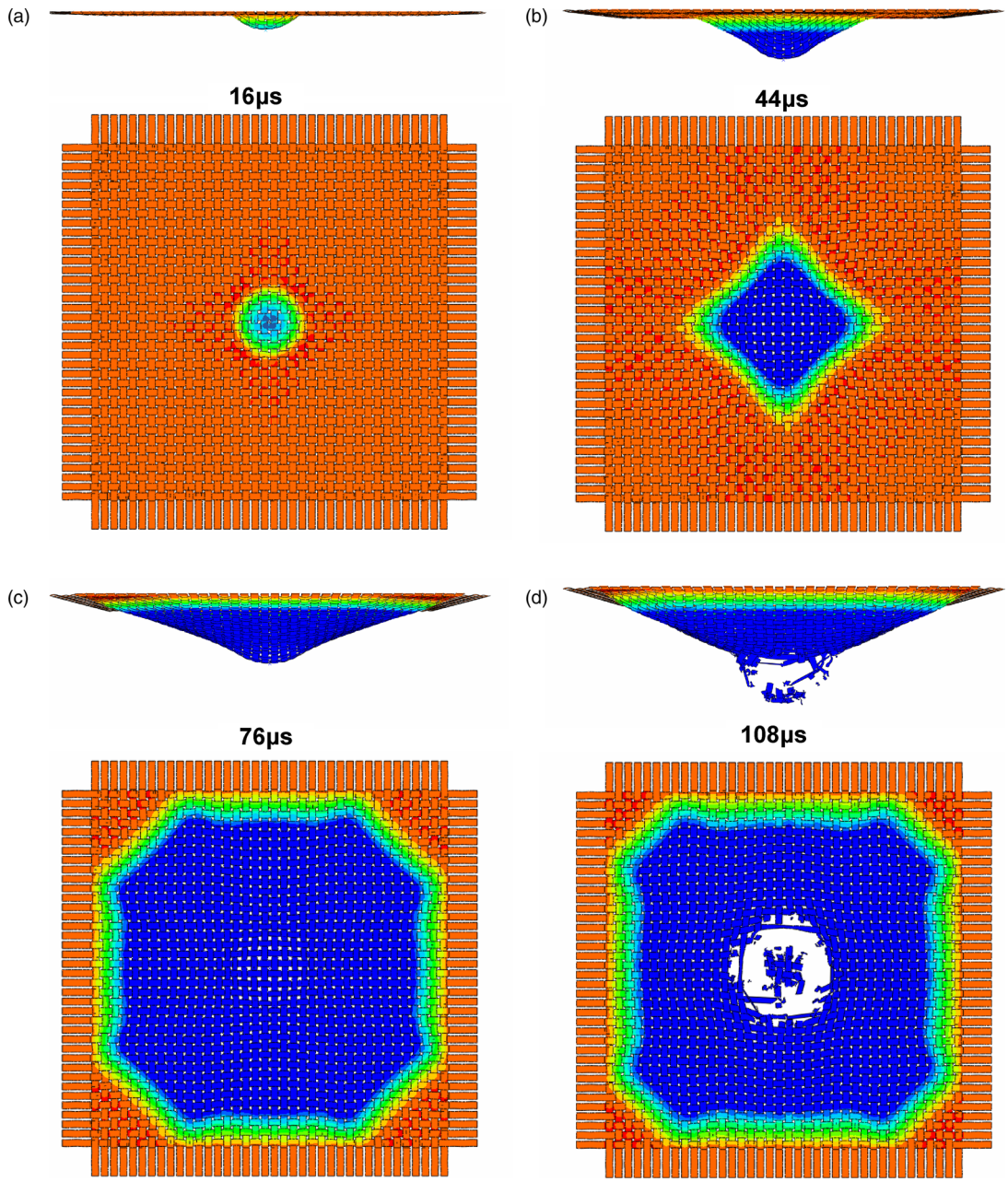

Fig. 4 The temporal evolution of deformation in the fabric for the membrane FEM model under the yarn–yarn and projectile–fabric friction-coefficient conditions of 0.5. Contour bands correspond to different values of the transverse displacement, i.e. the displacements normal to the fabric surface

shown for brevity), as well as a quite larger failure region (i.e. a larger number of failed yarns is observed in the case of membrane FEM analysis (Fig. 4(d)).

5. It should be noted that despite the fact that the projectile–fabric model has two vertical planes of symmetry, the damage region is asymmetric in both types of analyses. The reason for this is that the finite-element discretization of the projectile into tetrahedron elements used in this work does not possess two planes of symmetry. The results displayed in Figs 3 and 4 thus also reveal the effect of small geometrical perturbations in the (spherical) projectile on the fabric failure response.
6. Upon its penetration by the projectile, the fabric recoils and the final shape of its transversely-deflected zone becomes near conical.

The results displayed in Figs 3 and 4 and their discussion aforesaid clearly establish that, at the yarn–yarn and projectile–yarn friction-coefficient conditions of 0.5, the two FEM analyses yield comparable results regarding the temporal evolution of the deformation within the fabric during impact. However, some discrepancies were observed relative to the extent of fabric damage and the presence/absence of the fabric-corner failure mode. Similar observations were made in the case of the three other frictional conditions studied here. For brevity, only the results corresponding to zero yarn–yarn and projectile–fabric friction conditions are displayed (Figs 5 and 6) and discussed here. A simple comparison of the results displayed in Figs 3 and 4 with the corresponding results shown in Figs 5 and 6 established the following important observations.

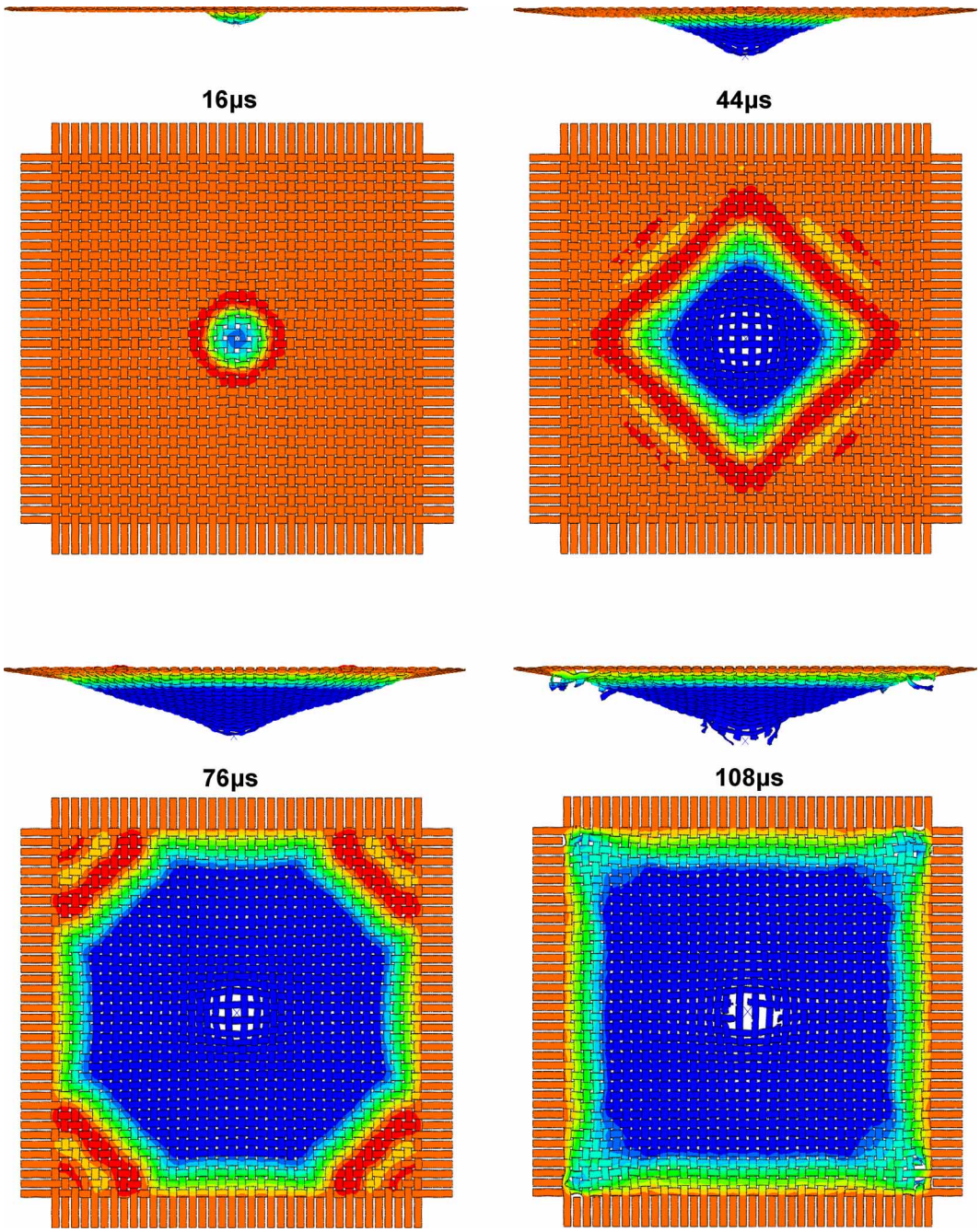

Fig. 5 The temporal evolution of deformation in the fabric for the solid FEM model in the absence of yarn–yarn and projectile–fabric friction. Contour bands correspond to different values of the transverse displacement, i.e. the displacements normal to the fabric surface

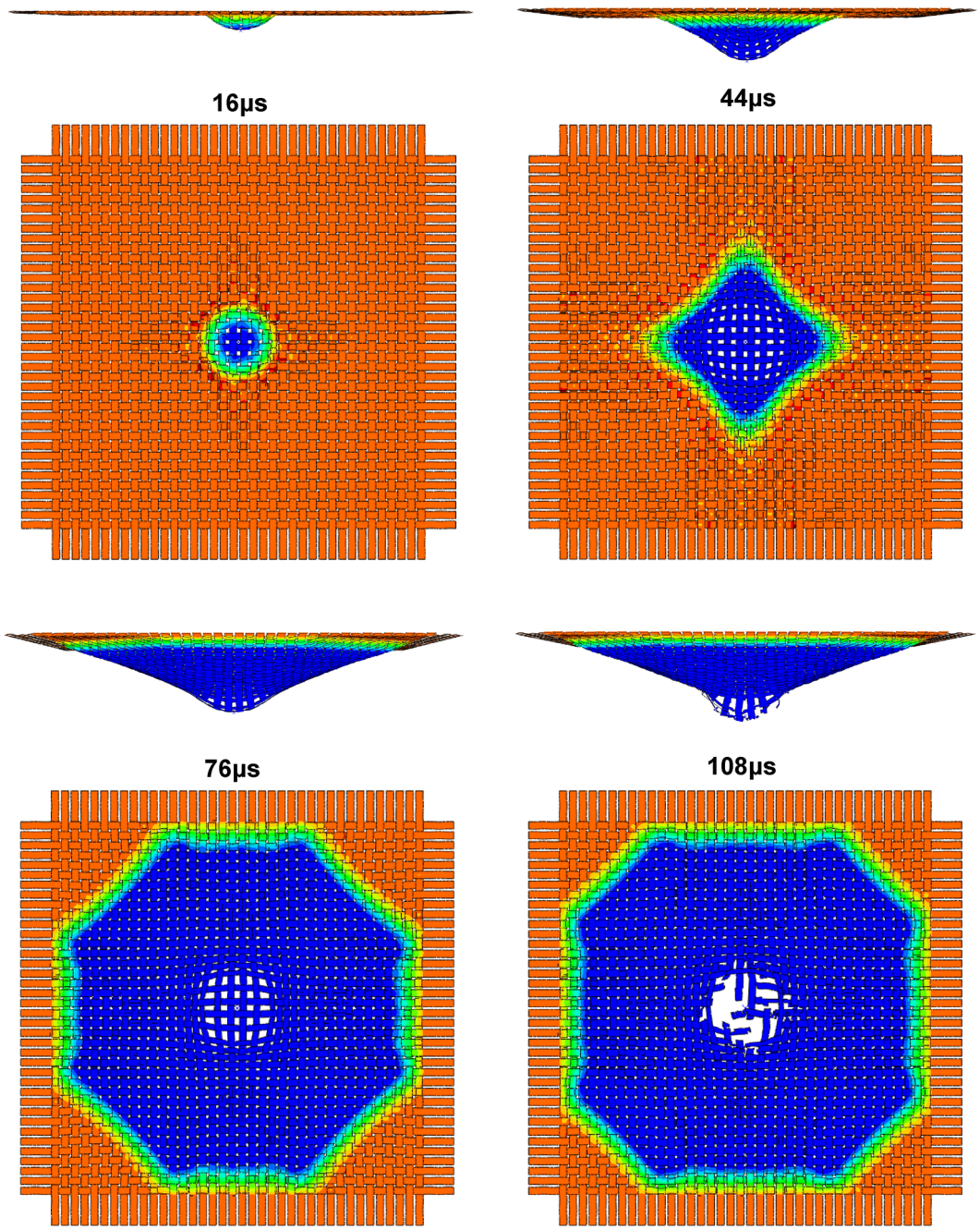

Fig. 6 The temporal evolution of deformation in the fabric for the membrane FEM model in the absence of yarn–yarn and projectile–fabric friction. Contour bands correspond to different values of the transverse displacement, i.e. the displacements normal to the fabric surface

1. No significant changes are introduced in the temporal evolution and the spatial distribution of the transverse-deflection wave due to elimination of the yarn–yarn and the projectile–fabric friction.
2. The structure of the fabric (including its deformation and failure) in the impact region and in the nearby surrounding regions is greatly affected in the case of zero yarn–yarn and projectile–fabric friction conditions. Specifically, in the zero-friction case, yarns were substantially displaced in the in-plane directions away from the centre of impact. This finding can be readily explained by the fact that the friction at the yarn crossovers provides resistance to the relative tangential motion of the yarns, while such resistance is absent in the zero-friction case. Consequently, in the zero-friction case yarns impacted by the projectile are pushed outward, a fewer number of yarns are broken and the projectile manages to penetrate the fabric mainly by '*wedging*' through it.

The temporal evolution of deformation and failure state of the fabric for the remaining two frictional conditions were found to be similar to those displayed in Figs 3 to 6 and the structure of the fabric in the impact region and in the nearby surrounding regions was more affected than in the $\mu_{y/y} = \mu_{p/f} = 0.5$ case and less affected relative to the zero-friction case. No significant differences in the fabric structure could be established between the $\mu_{y/y} = 0/\mu_{p/f} = 0.5$ case and the $\mu_{y/y} = 0.5/\mu_{p/f} = 0$ case.

The effect of the yarn–yarn and projectile–fabric frictional conditions on the fabric failure pattern at the moment of complete fabric penetration by the projectile is displayed in Figs 7(a) to (d) and 8(a) to (d) for the cases of the solid and the membrane FEM analyses, respectively. The results displayed in these figures clearly establish the following points.

1. The type of (solid versus membrane) of FEM analysis used clearly affects the predicted damage pattern of the fabric for each of the four yarn–yarn and projectile–fabric frictional conditions. Specifically, the size of the penetration hole and the number of yarns broken under given frictional conditions at the yarn–yarn crossovers and the projectile–fabric contact surface is larger in the case of the membrane FEM analysis. This is clearly seen by comparing the zero-friction results displayed in Figs 7(b) and 8(b) where it is seen that two vertical principal yarns in the case of the solid FEM analysis remain unbroken, Fig. 7(b), while all principal yarns are broken in the case of the membrane FEM analysis, Fig. 8(b).
2. The size of the penetration hole and the number of broken yarns are both increased in the presence of yarn–yarn and projectile–fabric friction. This observation can be linked to the fact that friction at yarn crossovers creates resistance to the relative motion between the contacting principal and secondary yarns, while the presence of projectile–fabric friction hampers in-plane outward deflection of the principal yarns. Consequently, yarns impacted by the projectile become loaded/strained and ultimately break. In the absence of friction, yarns are able to easily slip past each other and slip pass the projectile during the impact. As a result, fewer yarns become strained up to the point of fracture. Furthermore, the yarns that escaped the projectile can

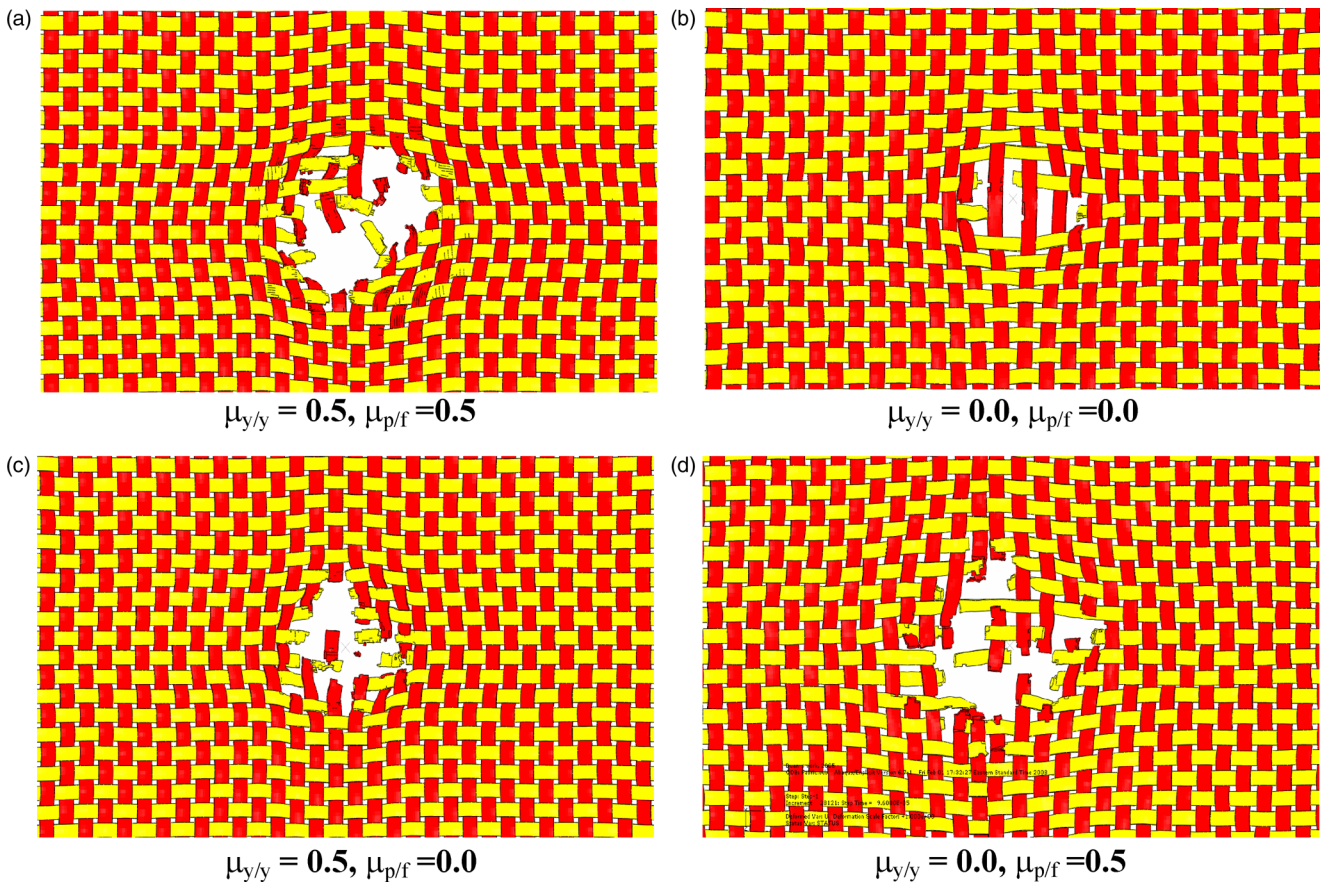

Fig. 7 The effect of yarn–yarn $\mu_{y/y}$ and projectile–fabric $\mu_{p/f}$ friction coefficients on the failure pattern in the fabric for the case of the solid FEM model

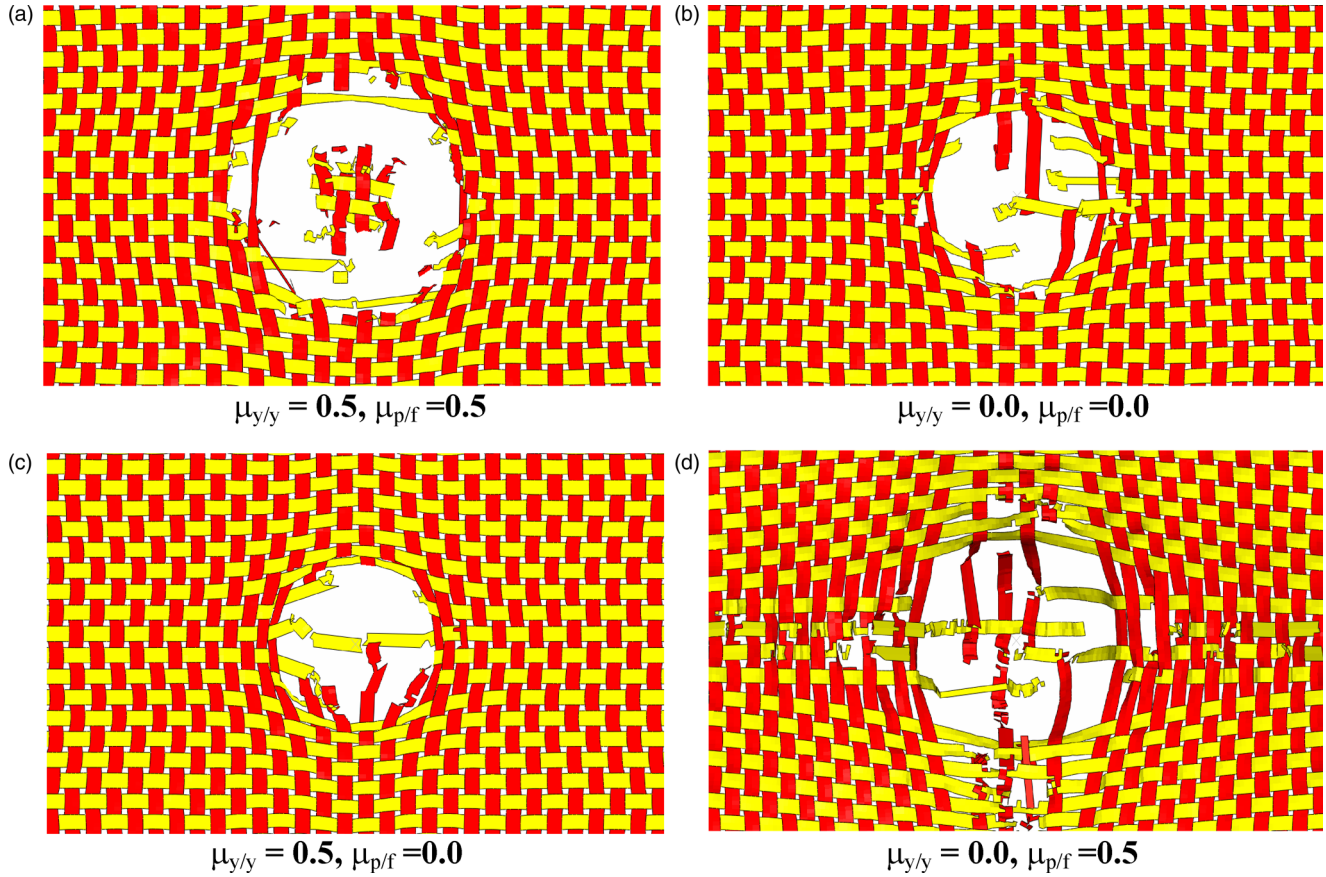

Fig. 8 The effect of yarn–yarn $\mu_{y/y}$ and projectile–fabric $\mu_{p/f}$ friction coefficients on the failure pattern in the fabric for the case of the membrane FEM model

relax more toward their initial position, making the final size of the penetration hole smaller.

3. The size of the penetration hole and the number of broken yarns are both reduced in the case when either yarn–yarn or projectile–yarn friction are absent, are found to be between their counterparts in the $\mu_{y/y} = \mu_{p/f} = 0.5$ and $\mu_{y/y} = \mu_{p/f} = 0$ cases. For both the solid and the membrane FEM analyses, friction at the projectile–fabric contact surface appears to have a more pronounced effect than inter-yarn friction. This can be readily established by starting from the $\mu_{y/y} = \mu_{p/f} = 0$ case, Figs 7(b) and 8(b), and adding projectile–fabric and yarn–yarn friction, one at a time (Figs 7(c) to (d) and 8(c) to (d), respectively).

3.1.2 Energy absorption capacity of the fabric

Temporal evolution of the three main components of the absorbed energy (i.e. yarn deformation energy, the fabric kinetic energy, and the frictional sliding energy), of a sum of these three components, and of the total loss in the projectile kinetic energy for the two types of simulations, the yarn–yarn and projectile–fabric frictional coefficients of 0.5, are displayed in Figs 9(a) and 10(a), respectively. The corresponding plots obtained under zero friction conditions (no frictional sliding energy term appears in this case) are displayed in Figs 9(b) and 10(b). It should be noted that all the absorbed-energy components displayed in these figures are normalized with respect to the maximum value of projectile kinetic energy loss in the case at hand. A simple analysis of the results displayed in Figs 9(a) to (b) and 10(a) to (b) reveals the following points.

1. No significant differences (typically <5 per cent) in the corresponding final values of the total projectile kinetic-energy loss and in the corresponding final values of the three different absorbed-energy components. More significant differences are seen in temporal evolutions of these quantities. These differences can be linked to the associated differences in the yarn–yarn and projectile–fabric contact-zone geometries. The latter differences are caused by the fact that, in the case of the solid FEM analysis, the side-truncated sinusoidal yarn cross-section was represented explicitly using a six-element wide fine mesh, while in the case of the membrane FEM analysis, the same cross-section was approximated

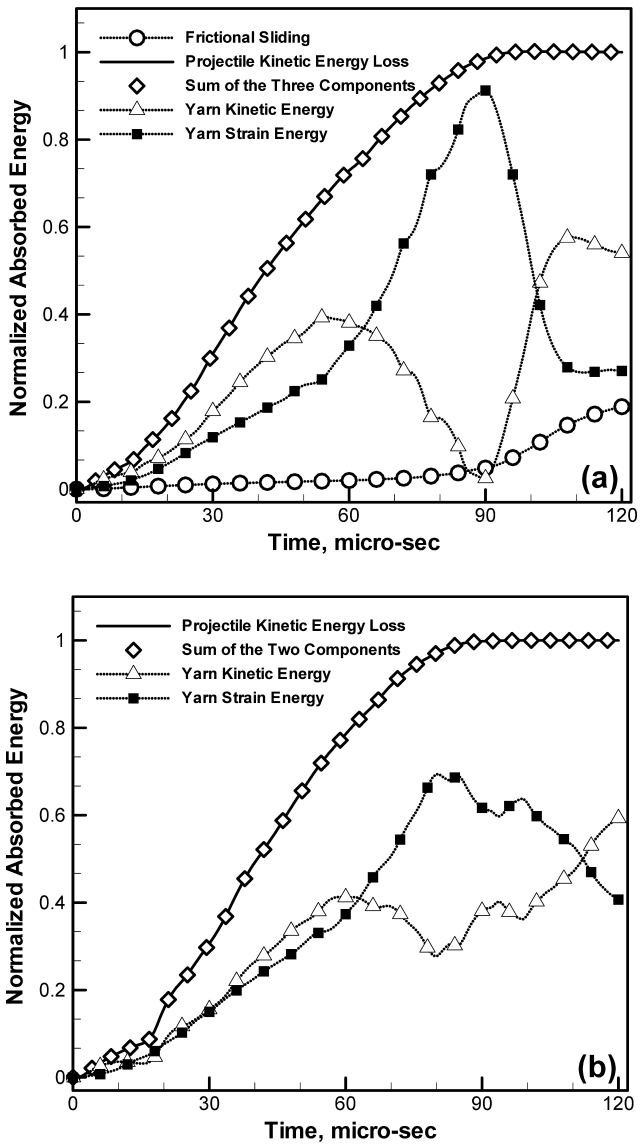

Fig. 9 The effect of yarn–yarn $\mu_{y/y}$ and projectile–fabric $\mu_{p/f}$ friction coefficients on the temporal evolution of projectile's kinetic-energy loss and on different energy-absorbing mechanisms in the fabric obtained using the solid FEM model: (a) $\mu_{y/y} = \mu_{p/f} = 0.5$ and (b) $\mu_{y/y} = \mu_{p/f} = 0.0$

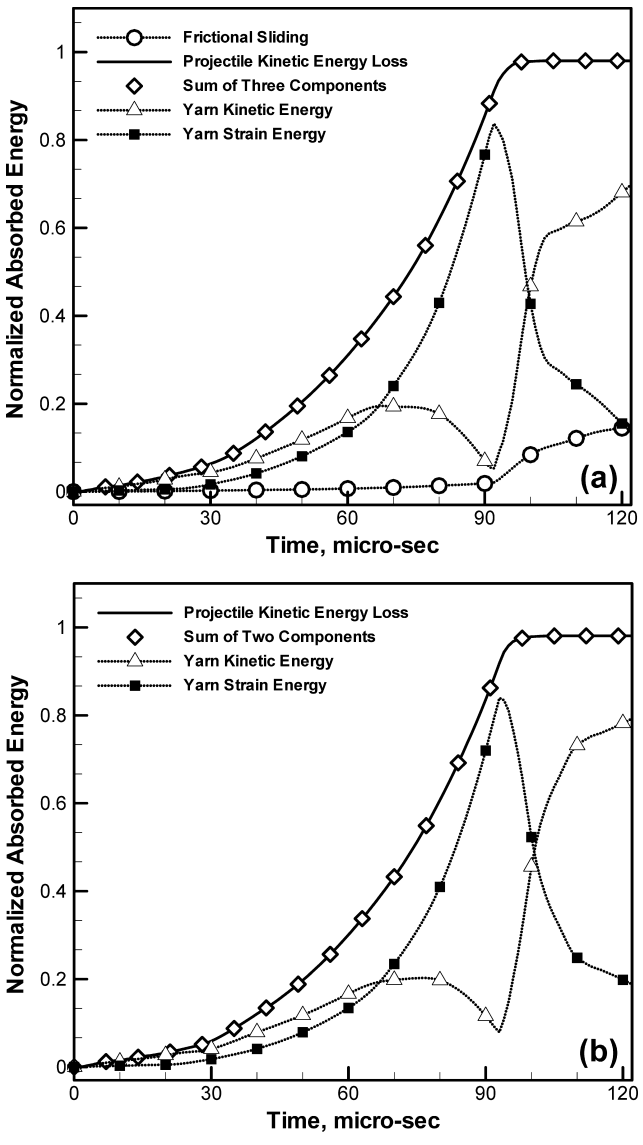

Fig. 10 The effect of yarn–yarn $\mu_{y/y}$ and projectile–fabric $\mu_{p/f}$ friction coefficients on the temporal evolution of projectile's kinetic energy loss and on different energy-absorbing mechanisms in the fabric obtained using the membrane FEM model: (a) $\mu_{y/y} = \mu_{p/f} = 0.5$ and (b) $\mu_{y/y} = \mu_{p/f} = 0.0$

using a two-element wide hexagon and a nodal thickness option. Consequently, the geometry of the projectile–yarn contact interface defined in terms of slave nodes of the projectile outer surface and the master element based surface of the fabric is quite different in the two analyses.

2. The sum of the three absorbed-energy components is equal to the total kinetic energy loss by the projectile, i.e. strain energy of the fabric, the fabric kinetic energy, and frictional sliding losses at yarn–yarn crossovers and projectile–fabric contact surfaces are indeed the primary modes of energy absorption by the fabric.
3. Initially (till ~60–65 μs), the contributions of the yarn strain energy and the yarn kinetic energy to the energy-absorption capacity of the fabric are comparable.
4. At longer impact times, however, the yarn strain energy becomes the more dominant mechanism of energy absorption. Relative increase in the strain-energy contribution continues until its peak, which coincides with the breakage of yarns.
5. Before yarn breaking, the fabric absorbs between ~80 and 90 per cent of the total projectile kinetic-energy loss. The remainder of the energy absorption

takes place after yarn breaking, i.e. during the fabric perforation process.

6. Past the point of yarn breaking, yarn strain energy undergoes a sharp drop. This is caused by its conversion into fabric kinetic energy and the frictional sliding losses.
7. While initial contributions of the frictional-sliding energy losses to the total energy-absorption capacity of the fabric are quite small, during the fabric perforation stage, this mechanism of energy absorption becomes more important.
8. The presence of yarn–yarn and projectile–fabric friction affects the total energy absorbing potential of the fabric. Namely, the projectile kinetic-energy losses corresponding to the '*Normalized Absorbed Energy*' of 1.0 in Figs 9(a) and 10(a), is higher by 5–7 per cent than their counterparts in Figs 9(b) and 10(b).
9. The presence of yarn–yarn and projectile–fabric friction not only affects the frictional-sliding energy loss contribution (the contribution which is relatively small) but also increases the contributions of the yarn strain energy and the fabric kinetic energy to the fabric energy absorption capacity. This finding is related to the aforementioned increased coupling among the yarns in the presence of friction.

To help further explain the aforementioned effect of yarn–yarn friction and projectile–fabric friction on the energy-absorption potential of the fabric, the extent of yarn stressing is next investigated. Toward that end, distributions of the von Mises equivalent stress in the fabric are computed and displayed in Figs 11(a) and (b) for the $\mu_{y/y} = \mu_{p/f} = 0.5$ and $\mu_{y/y} = \mu_{p/f} = 0$ conditions, respectively. The results displayed in Figs 11(a) and (b) were obtained using the membrane FEM analysis. Similar results (not shown for brevity) were obtained using the solid FEM analysis. A simple analysis of the results displayed in Figs 11(a) and (b) reveals that stress is primarily located within the principal yarns and that a larger number of yarns are stressed in the case when friction is present at the yarn–yarn and projectile–fabric contact surfaces.

These differences are associated with the fact that due to frictional effects, yarn motion is more constrained, leading to a more effective load transfer among the yarns. This in turn leads to more yarns being loaded and absorbing energy through deformation. Along the same yarn, resistance to the relative motion of yarns with respect to other yarns and with respect to the projectile causes more yarns to be accelerated in the projectile-motion direction, leading to a higher kinetic-energy contribution to the fabric energy-absorption capacity.

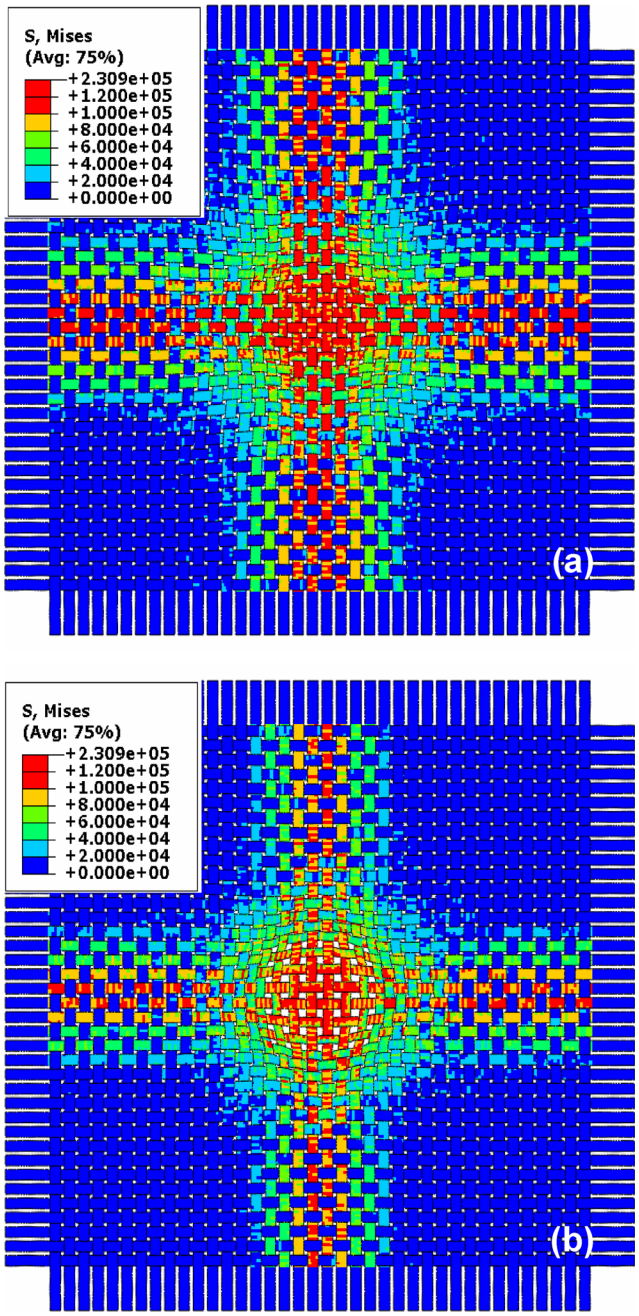

Fig. 11 The effect of yarn–yarn $\mu_{y/y}$ and projectile–fabric $\mu_{p/f}$ friction coefficients on the spatial distribution of the von Mises equivalent stress within the fabric: (a) $\mu_{y/y} = \mu_{p/f} = 0.5$ and (b) $\mu_{y/y} = \mu_{p/f} = 0.0$

3.1.3 *Separating the roles of yarn–yarn friction and projectile–fabric friction*

In the previous section, two types of FEM analyses of the projectile–fabric interactions were examined under either the same non-zero yarn–yarn or projectile–fabric frictional conditions or in the absence of such friction. While the results displayed

revealed that friction plays an important role in the deformation and fracture response of the fabric and in its ability to absorb the kinetic energy carried by the projectile, the analyses carried out in the previous section were not able to separate the yarn–yarn and projectile–fabric frictional contributions. Therefore, in this section two additional frictional conditions are considered: (a) zero yarn–yarn friction and 0.5 projectile–fabric friction coefficients, and (b) zero projectile–fabric and 0.5 yarn–yarn friction coefficient.

Figures 12(a) and (b) shows the temporal evolutions of the energy-absorption capacity of the fabric for the four frictional conditions considered in this work and for the two types of FEM analyses, respectively. In each case, the results are normalized with respect to the overall energy absorbed by the fabric (i.e. the projectile

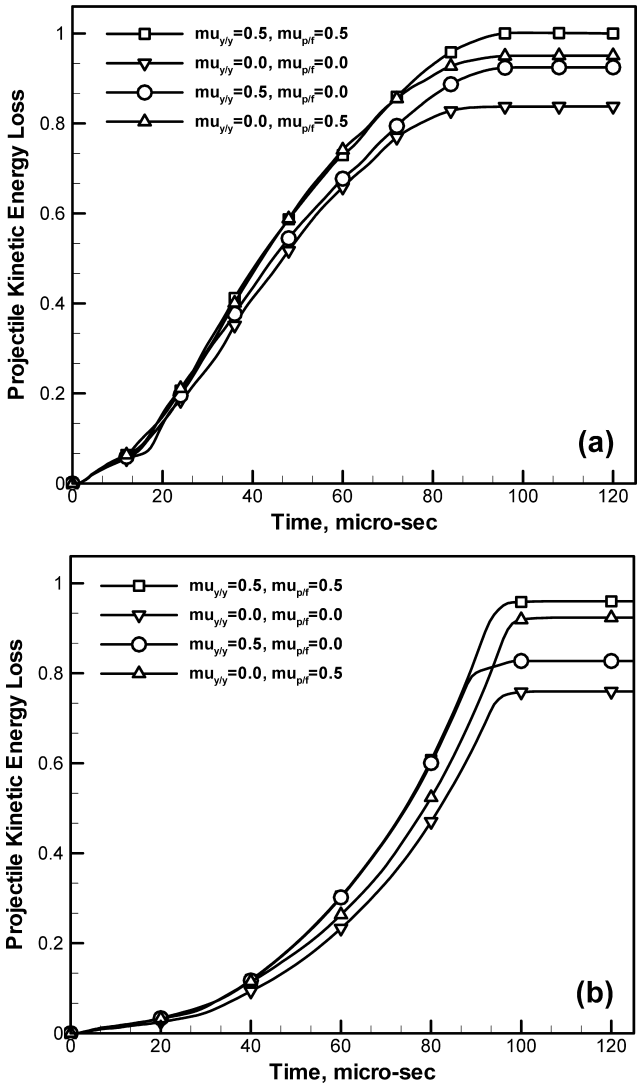

Fig. 12 The effect of the four different yarn–yarn frictional conditions on the energy-absorbing capacity of the fabric: (a) the solid FEM model and (b) the membrane FEM model

kinetic-energy loss) in the solid FEM analysis under yarn–yarn $\mu_{y/y}$ and projectile–fabric $\mu_{p/f}$ friction coefficients of 0.5. The results displayed in Figs 12(a) and (b) clearly established the following points.

1. The corresponding predictions regarding the temporal evolution of the absorbed energy are very comparable in the two types of FEM analyses.
2. Relative to the zero yarn–yarn and projectile–fabric frictional conditions, the yarn–yarn friction increases the final energy absorbed by ∼10–12 per cent, while the projectile–fabric friction increases the energy absorbed by ∼12–15 per cent.

It should be noted that while both yarn–yarn and projectile–fabric frictions are present, the fabric energy-absorption capacity is increased by ∼18–22 per cent, suggesting that simple linear superposition cannot be applied for the types of frictions.

The aforementioned effects of the yarn–yarn and projectile–fabric frictions can be explained as follows.

1. Yarn–yarn friction at the crossovers restricts the relative tangential motion of the yarns, helping maintain the integrity of the fabric.
2. Likewise, projectile–fabric friction restricts the lateral motion of the principal yarns that are, consequently, forced to remain in contact with the projectile.
3. For both the cases (1) and (2), the final outcome is that more yarns are being loaded/strained and accelerated, which increases the overall energy-absorption capacity of the fabric.

To further help separate the effects of the yarn–yarn and projectile–fabric frictions on the fabric's energy-absorption capacity, contributions of the three energy absorbing mechanisms are compared for the ($\mu_{y/y} = 0.5$)/($\mu_{p/f} = 0$) case and the $\mu_{y/y} = \mu_{p/f} = 0$ case (the results not shown for brevity). It is found that that the presence of friction at the projectile–fabric interfaces provides a substantial contribution to the fabric's energy-absorption potential in the later stage of impact. To rationalize this finding, a close examination was made of the deformation fields, von Mises stress distributions and the extent of fabric damage (i.e. the number of yarns broken in the two cases). It is found that projectile–fabric friction improves the fabric's ability to absorb energy through several effects: (a) the impact load (i.e. the reaction force measured at the reference point of the rigid spherical projectile) is increased and its peak value occurs for a longer time causing a larger region of the fabric to contribute to the energy absorption via straining and acceleration; (b) high-magnitude von Mises stresses are present not only in the fabric region directly underneath the projectile (as is the case when projectile–fabric friction

is absent), but also in the surrounding regions; and (c) consequently, a larger number of yarns get broken before full perforation of the projectile takes place.

It should also be noted that under some circumstances, the largest energy absorption of the fabric is attained when the projectile–fabric friction is present but no friction exist at the yarn–yarn crossover. This finding was rationalized as follows: due to the absence of yarn–yarn friction, broken yarns can readily recoil and de-crimp after breakage, causing a reduction in fabric tightness. This in turn increased the mobility of the unbroken yarns (located below the projectile allowing them to undergo more deformation and acquire more kinetic energy before their failure).

It should be recognized that the values of the yarn–yarn and the projectile–fabric frictional coefficients of 0.5 are rather high. Furthermore, under dynamic conditions the frictional coefficients should be further reduced. Hence, all the conclusions made here regarding the effect of friction pertain to an '*Upper-Bound*' friction case.

3.2 The effect of far-field boundary conditions

As explained earlier, three types of far-field boundary conditions were investigated: (a) all four fabric edges clamped; (b) two opposite fabric edges clamped and two others free; and (c) the four fabric corner nodes fixed and the remainder of the fabric edges free. In the previous section, a detailed account of the results is presented for the case of all four fabric edges being fixed. Due to space limitations, in this section only a brief summary of the results obtained under the two other boundary conditions is presented. The main finding relative to the initially stated objective of this work is that for the other two boundary conditionsalso, the two FEM analyses yielded very comparable results. The level of agreement of the corresponding results obtained in the two analyses were very similar to the one observed in the previous section.

In general, the choice of far-field boundary conditions applied along the edges of the fabric is found to have a profound effect on the temporal evolution and spatial distribution of deformation and damage within the fabric and on the fabric's energy-absorption capacity. These differences could be readily related to the fact that the longitudinal strain–stress wave that is generated at the centre of impact zone and moves outward toward the fabric edges reacts differently with the clamped and free edges. That is, in the case of clamped edges, the longitudinal waves are reflected back toward the centre of the impact zone and the strain (in the region of the fabric swept by the reflected wave) is doubled. In sharp contrast, when the longitudinal wave reaches free fabric edges, the strain within the fabric carried by the wave vanishes and the fabric begins to move longitudinally toward the impact region. Furthermore, due to yarn–yarn interactions, the free fabric edges do not remain straight but rather, tend to bow toward the centre of the impact zone. These differences also affected propagation of the transverse deflection wave. That is, due to attendant larger yarn strains in the case of clamped edges, the transverse wave tends to propagate faster along the clamped yarns than along the unclamped yarns.

The type of boundary conditions applied along the fabric edges is found to affect significantly the ability of the fabric to absorb the projectile's kinetic energy. More specifically, 3–6 and 6–10 per cent more kinetic energy is absorbed by the fabric when all four edges are clamped relative to the cases when two edges are clamped and no edges are clamped, respectively. Also, the role of friction was affected by the type of boundary conditions applied. That is, it is typically found that under all four edges free boundary conditions, friction provides more contribution to the energy absorption through the frictional sliding mechanism. In sharp contrast, in the case of two edges clamped and in particular, in the case of all edges being clamped, friction caused resistance to the lateral motion of the yarns, promoting their deformation and acceleration in the direction of projectile motion. In other words, friction increased the contributions of the strain energy and fabric kinetic energy to the energy-absorption potential of the fabric.

3.3 The effect of projectile geometry

Few selected analyses were carried out to establish if the type (solid versus membrane) of FEM analysis significantly affects results when a projectile of a different geometry is used. Toward that end, the 4 mm radius spherical projectile is replaced with a right circular cylinder with equal diameter and height of ∼9 mm. The two projectiles have identical volumes/weights. Due to space limitations, the results pertaining to the ballistic impact of the right circular cylindrical projectile with the fabric is displayed but is briefly discussed in this section.

In general, the level of agreement between the corresponding results obtained in the previous section for the spherical projectile is also seen in the case of the cylindrical projectile. The fabric's ability to absorb the kinetic energy of the projectile was found to be slightly (10–15 per cent) higher in the case of the cylindrical projectile. This observation was related to the larger contribution to the energy absorption arising from friction at the projectile–fabric contact surface. Since the projectile–fabric contact surface area is larger (particularly in the early stage of impact) in the case of the cylindrical projectile, more yarns are impacted

and constrained from moving laterally in the case of the cylindrical projectile. One noticeable difference between the fabric-failure pattern in the case of the spherical and cylindrical projectiles was also observed. That is, in the case of the spherical projectile, yarn failure was primarily localized near the centre of impact. In sharp contrast, in the case of the cylindrical projectile, failure near the periphery of the projectile was observed. These differences were related to the observed differences in the spatial distribution of the von Mises equivalent stress in the two cases. Namely, peaks in the von Mises equivalent stress are found near the periphery of the cylindrical projectile.

4 SUMMARY AND CONCLUSIONS

A set of two transient non-linear dynamic analyses pertaining to the ballistic impact of a rigid spherical projectile with a plain-woven balanced single-ply square-shaped textile-armour is carried out. The two analyses are different with respect to the geometrical representation of the yarns. In the first analysis, yarns are constructed using first-order eight-node solid elements, while in the second analysis second-order eight-node membrane elements are used. The objective of this work was to verify if the computationally more efficient membrane FEM analysis can be used in place of the more accurately solid FEM analysis and yet yield reliable results. Based on the results obtained in this work the following main conclusions can be drawn.

1. The two sets of analyses were found to yield quite comparable results under a variety of conditions such as yarn–yarn and projectile–fabric frictional conditions and under different far-field boundary conditions applied along the edges of the fabric. This finding is particularly true with respect to the temporal evolution and spatial distribution of transverse displacements in the fabric and the overall energy-absorbing capacity of the fabric armour.
2. In general, a five- to six-fold increase in the computational efficiency was found through the use of the membrane type FEM analysis.
3. Frictional conditions present at the yarn–yarn crossovers and at the projectile–fabric contact surface significantly affect the deformation history of the fabric and its ability to absorb the kinetic energy of the projectile and, in turn, on the energy-absorption efficiency of the fabric.
4. Far-field (fixed versus free) boundary conditions applied along the edges of the fabric are also found to have significant effect on the temporal evolution and spatial distribution of deformation and damage within the fabric and, in turn, on the ability of fabric to absorb the projectile's kinetic energy.
5. The shape (spherical versus right circular cylinder) of the projectile was not found to affect the computational results obtained in this work to any significant extent.

ACKNOWLEDGEMENTS

This work was supported by the US Army/Clemson University Cooperative Agreements W911NF-04-2-0024 and W911NF-06-2-0042. The authors are indebted to Dr Fred Stanton for the support and a continuing interest in this work.

REFERENCES

1 **Roylance, D.** and **Wang, S. S.** *Penetration mechanics of textile structures, ballistic materials and penetration mechanics*, 1980, pp. 273–292 (Elsevier, Amsterdam).
2 **Shim, V. P. W., Lim, C. T.,** and **Foo, K. J.** Dynamic mechanical properties of fabric armour. *Int. J. Impact Eng.*, 2001, **25**, 1–15.
3 **Lim, C. T., Shim, V. P. W.,** and **Ng, Y. H.** Finite element modeling of the ballistic impact of fabric armor. *Int. J. Impact Eng.*, 2003, **28**, 13–31.
4 **Shahkarami, A., Vaziri, R., Poursartip, A.,** and **Williams, K.** A numerical investigation of the effect of projectile mass on the energy absorption of fabric panels subjected to ballistic impact. In Proceedings of the 20th International Symposium on *Ballistics*, Orlando, FL, 2002, pp. 802–809.
5 **Johnson, G. R., Beissel, S. R.,** and **Cunniff, P. M.** A computational model for fabrics subjected to ballistic impact. In Proceedings of the 18th International Symposium on *Ballistics*, San Antonio, 1999, vol. 2, pp. 962–969.
6 **Billon, H. H.** and **Robinson, D. J.** Models for the ballistic impact of fabric armour. *Int. J. Impact Eng.*, 2001, **25**, 411–422.
7 **Shockey, D. A., Erlich, D. C.,** and **Simons, J. W.** *Improved barriers to turbine engine fragments*. US department of Transportation, 2000 (SRI International, Menlo Park, California).
8 **Duan, Y., Keefe, M., Bogetti, T. A.,** and **Cheeseman, B. A.** Modeling friction effects on the ballistic impact behavior of a single-ply high-strength fabric. *Int. J. Impact Eng.*, 2005, **31**, 996–1012.
9 **Duan, Y., Keefe, M., Bogetti, T. A.,** and **Cheeseman, B. A.** Modeling the role of friction during ballistic impact of a high-strength plain-weave fabric. *Int. Compos. Struct.*, 2005, **68**, 331–337.
10 **Duan, Y., Keefe, M., Bogetti, T. A., Cheeseman, B. A.,** and **Powers, B.** A numerical investigation of the influence of friction on energy absorption by a high-strength fabric subjected to ballistic impact. *Int. J. Impact Eng.*, 2006, **32**, 1299–1312.
11 **Duan, Y., Keefe, M., Bogetti, T. A.,** and **Powers, B.** Finite element modeling of transverse impact on a ballistic fabric. *Int. J. Mech. Sci.*, 2006, **48**, 33–43.

12 **Zhang, G. M., Batra, R. C.,** and **Zheng, J.** Effect of frame size, frame type, and clamping pressure on the ballistic performance of soft body armor. *Compos. B*, in press.
13 **Kawabata, S., Niwa, M.,** and **Kawai, H.** The finite-deformation theory of plain-weave fabrics part I: the biaxial-deformation theory. *J. Text. Inst.*, 1973, **64**, 21–46.
14 **Kawabata, S., Niwa, M.,** and **Kawai, H.** The finite-deformation theory of plain-weave fabrics. Part II. The uniaxial-deformation theory. *J. Text. Inst.*, 1973, **64**, 47–61.
15 **Kawabata, S., Niwa, M.,** and **Kawai, H.** The finite-deformation theory of plain-weave fabrics. Part I. The shear-deformation theory. *J. Text. Inst.*, 1973, **64**, 62–85.
16 **Ivanov, I.** and **Tabiei, A.** Loosely woven fabric model with viscoelastic crimped fibres for ballistic impact simulations. *Int. J. Numer. Methods Eng.*, 2004, **61**, 1565–1583.
17 **King, M. J., Jearanaisilawong, P.,** and **Socrate, S.** A continuum constitutive model for the mechanical behavior of woven fabrics. *Int. J. Solids Struct.*, 2005, **42**, 3867–3896.
18 **Boisse, P., Zouari, B.,** and **Gasser, A.** A mesoscopic approach for the simulation of woven fibre composite forming. *Compos. Sci. Technol.*, 2005, **65**, 429–436.
19 **Peng, X.** and **Cao, J.** A dual homogenization and finite element approach for material characterization of textile composites. *Compos. B, Eng.*, 2002, **33**, 45–56.
20 **Shahkarami, A.** and **Vaziri, R.** A continuum shell finite element model for impact simulation of woven fabrics. *Int. J. Impact Eng.*, 2007, **34**, 104–119.
21 **Scott, B. R.** and **Yen, C. F.** Analytic design trends in fabric armor. In Proceedings of the 22nd International Ballistics Symposium, Vancouver, Canada, 2005, pp. 752–760.
22 *ABAQUS version 6.7. User documentation*, 2007 (Dessault Systems).
23 **Starratt, D., Sanders, T., Cepus, E., Poursartip, A.,** and **Vaziri, R.** An efficient method for continuous measurement of projectile motion in ballistic impact experiments. *Int. J. Impact Eng.*, 2000, **24**, 155–170.
24 **Cheeseman, B. A.** and **Bogetti, T. A.** Ballistic impact into fabric and compliant composite laminates. *Compos. Struct.*, 2003, **61**, 161–173.
25 **Tan, V. B. C., Lim, C. T.,** and **Cheong, C. H.** Perforation of high-strength fabric by projectiles of different geometry. *Int. J. Impact. Eng.*, 2003, **28**, 207–222.